NMR study comparing the electronic structures of ZrH_x and TiH_x

C. Korn
*Laboratory of Atomic and Solid State Physics, Cornell University, Ithaca, New York 14853 and Department of Physics, Ben Gurion University of the Negev, Beer Sheva, 84 120 Israel**
(Received 2 September 1982)

The temperature and concentration dependences of the proton spin-lattice relaxation time T_1, Knight shift K, and the lattice parameters were obtained for zirconium and titanium hydride samples having a wide variety of concentrations at temperatures where the relaxation rate was due primarily to interaction with the conduction electrons. A sharp peak in $(T_1T)^{-1/2}$ was found at $ZrH_{1.80}$ and $TiH_{1.92}$, while the tetragonal distortion occurred at lower concentrations. $(T_1T)^{-1/2}$ changed continuously across the tetragonal transition. The results are compared with recent band-structure calculations. The dominant proton hyperfine field was attributed to core polarization and the hyperfine field was estimated to be -13.5 kG. A correlation is noted whereby the microhardness of ZrH_x varies inversely with $(T_1T)^{-1/2}$.

I. INTRODUCTION

Zirconium lies directly below titanium in the Periodic Table. It is thus not surprising that their hydrides display very similar properties. They both span a nonstoichiometric hydrogen concentration range of $x=1.5$ to 2 where the hydrides are designated by TiH_x and ZrH_x. In the lower part of this range the metal atoms form an fcc structure with the hydrogen randomly distributed among the tetrahedral sites, while at higher concentrations a tetragonal distortion with $c/a<1$ occurs. Despite these and other similarities the hydrides also display a number of differences. For example, the tetragonal distortion of zirconium hydride is much more severe and is retained to the highest measured temperatures (500 °C) while that of TiH_x reverts to the cubic structure above about 40 °C.[1] These and other properties have been ascribed in part to the electronic structure.

In this study, nuclear magnetic resonance (NMR) has been used to compare the electronic structures of the two hydrides. This technique has proven itself useful for TiH_x where it was employed for a small number of samples.[2] Here a much larger range of samples was used the results indicating that some of the previous extrapolations must be amended. Preliminary measurements showing a peak in the density of states at $x=1.8$ were reported for the ZrH_x system[3] and a more detailed study is given here. Subsequent to the present measurements an NMR investigation by Goring, Lucas, and Bohmhammel[4] appeared which overlaps some of the TiH_x portion of this work. Bowman and Rhim[5] used NMR to investigate the influence of V alloying on the TiH_x system while Nowak, Zogal, and Minier[6] did the same for Nb alloying. A number of other NMR studies of the TiH_x and ZrH_x systems emphasizing different aspects but yielding some parameters related to the electronics structure have been reported.[7–13]

In recent years many band-structure calculations of metal hydrides have appeared following the pioneering work of Switendick.[14] These include density-of-states (DOS) diagrams for the Ti-H and Zr-H systems[14–19] to which our results can be compared. Other measurements directly related to the density of states include the classical magnetic susceptibility results of Trzebiatowsky and Stalinski[20] for Ti-H, the magnetic susceptibility and low-temperature heat capacity for a few samples of Ti-H and Zr-H of Ducastelle, Caudron, and Costa,[21] and most recently, the low-temperature heat capacity for the Ti-H system of Bohmhammel, Wolf, Gross, and Madge.[22]

The proton spin-lattice relaxation time T_1 was measured as a function of hydrogen concentration at three different temperatures and the proton Knight shift K was obtained at room temperature for a large number of TiH_x and ZrH_x samples. The temperature dependence of T_1 for a number of ZrH_x samples was also obtained. As will be discussed later $(T_1T)^{-1/2}$ and K are related to the density of states. Since we wish to compare our results to the crystallographic structure, the lattice parameters were obtained for the same samples as were subjected to NMR. This is important due to a number of small

discrepancies found among various investigators that can often be attributed to differences in sample purity, accuracy in concentration determination, and heat treatment during sample preparation.

II. EXPERIMENTAL PROCEDURE

A. Sample preparation

ZrH_2 and TiH_2 powder was prepared from the metal sponge by direct absorption from the gas with the use of procedures previously outlined.[23] Pure Zr and Ti metal powder was obtained by outgassing the hydrides. Properly proportioned hydrides and pure metal were sealed into small-volume evacuated pyrex ampoules heated to 525 °C for about 20 days, then to 425 °C for an additional 2 days, and slowly cooled down. Since annealing of the hydrides can affect the behavior of the tetragonal distortion,[24] this homogenizing procedure resulted not only in a series of hydrides with different hydrogen concentrations, but also gave the proper annealing. Included in the series were two ampoules containing TiH_2 and ZrH_2 without any pure metal mixed in but subjected to the same heat treatment and two identical samples sealed off in ampoules but not subjected to the heat treatment. The latter will be referred to in the text as the unannealed samples and gave slightly different NMR results. Continuity considerations of our T_1 measurements at all three temperatures, Knight-shift measurements, and x-ray-diffraction measurements resulted in a relabeling of samples that should have been $TiH_{1.985}$ and $TiH_{1.973}$ to be $TiH_{1.928}$ and $TiH_{1.925}$. The original errors were probably due to incorrectly recording the weights. The number of Ti-H samples is large making this insignificant in any event. It is believed that the relative concentration determinations are meaningful to the third decimal place.

B. NMR measurements

T_1 measurements were performed using a Bruker B-KR321s pulsed spectrometer by flipping the spins with an initial 180° pulse and monitoring the subsequent signal amplitude as a function of time with the use of a boxcar integrator. The monitoring signal was usually obtained using a solid echo. T_1 was calculated with the use of a least-squares-fit analysis based on the method suggested by MacDonald.[25] Since we are attempting to study the electronic structure, we wish to minimize relaxation contributions resulting from hydrogen diffusion. The strength of this process is inversely proportional to the square of the resonance frequency for the lower temperatures which we employ here. Thus the highest feasible resonance frequency compatible with our instrumentation was used, namely 50 MHz. This also contributed to a better signal-to-noise ratio and a shortening of the recovery time.

Since the Knight shift is proportional to the resonance frequency, 50 MHz was also used for this measurement. The difficulty of measuring K in our case is that the shift is a small fraction of the linewidth. Bowman *et al.*[5] and Goring *et al.*[4] overcame this with the use of zero-crossing and multiple-pulse techniques. In this study the signal following a 90° pulse, phase shifted by 90° from the instrument reference signal, was observed. This is equivalent to looking at the dispersion signal in cw which goes through zero at resonance. It is much more accurate and simpler to find a null than a maximum. Resonance was first found for water. Then the sample was substituted and the frequency of the synthesizer was adjusted to give a straight horizontal line on the oscilloscope signifying the null. Care had to be employed since inserting the metallic hydride in the coil caused different phase shifts for different samples. The phase and frequency were adjusted until the signal was symmetric about the null when varying the frequency. A run consisted of measuring all the samples. In each run the ampoules were mixed in a box and selected randomly so as to eliminate subjective prejudice in favor of results from previous runs or trends in accordance to hydrogen concentration.

C. X-ray-diffraction measurements

The crystallographic measurements were performed on the powdered samples using the Debye-Scherrer technique and Ni-filtered Cu radiation. Systematic errors were minimized by obtaining a least-squares straight-line fit to the lattice parameters obtained from the deflections as a function of $F(\theta)=0.5(1/\sin\theta + 1/\theta)\cos^2\theta$ and extrapolating to $\theta=\pi/2$.[26]

III. EXPERIMENTAL RESULTS

A. Lattice parameters

Figures 1 and 2 show the room-temperature dependence of the lattice constants of the Zr-H and Ti-H systems as a function of hydrogen concentration. Standard usage assigned inconsistent designations for corresponding regions of the phase diagrams of Ti-H and Zr-H. Since we will be comparing the two systems, it is important to clarify the nomenclature. Below 100 °C both Ti and Zr dissolve negligible amounts of hydrogen in their original hcp structure. This is called the α phase. The hydride

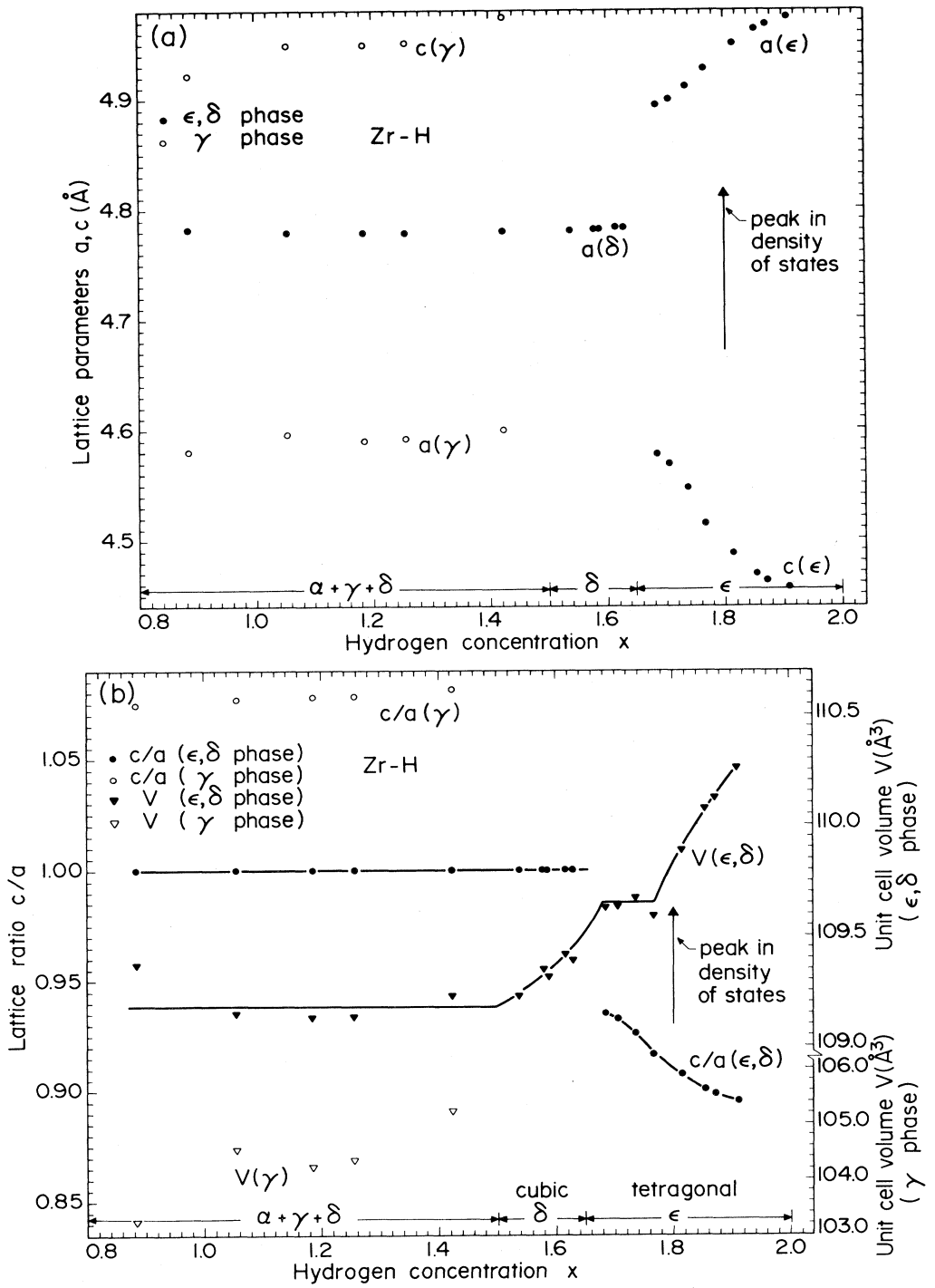

FIG. 1. Room-temperature lattice parameters of the Zr-H system showing the fcc δ phase, the fct ϵ phase, and the metastable fct γ phase in the α+γ+δ region. Arrows indicate concentration at which the peak in the DOS appears as inferred from NMR. (a) Hydrogen concentration dependence of a and c, and (b) hydrogen concentration dependence of c/a and unit-cell volume V. Note change of scale of V for the γ phase.

region between $x=1.5$ and 2.0 has two crystallographic forms: one is fcc in the lower-concentration region and the other is a tetragonally distorted fct region with $c/a<1$. For Zr-H the cubic region is called the δ phase and the tetragonal region is called the ϵ phase, while for Ti-H the cubic phase is referred to as γ and the tetragonal phase as δ. Thus for concentrations below $x=1.5$ in Ti-H there is a mixed α+γ region consisting of (almost) pure hcp Ti and cubic $TiH_{1.5}$, while for Zr-H there should be

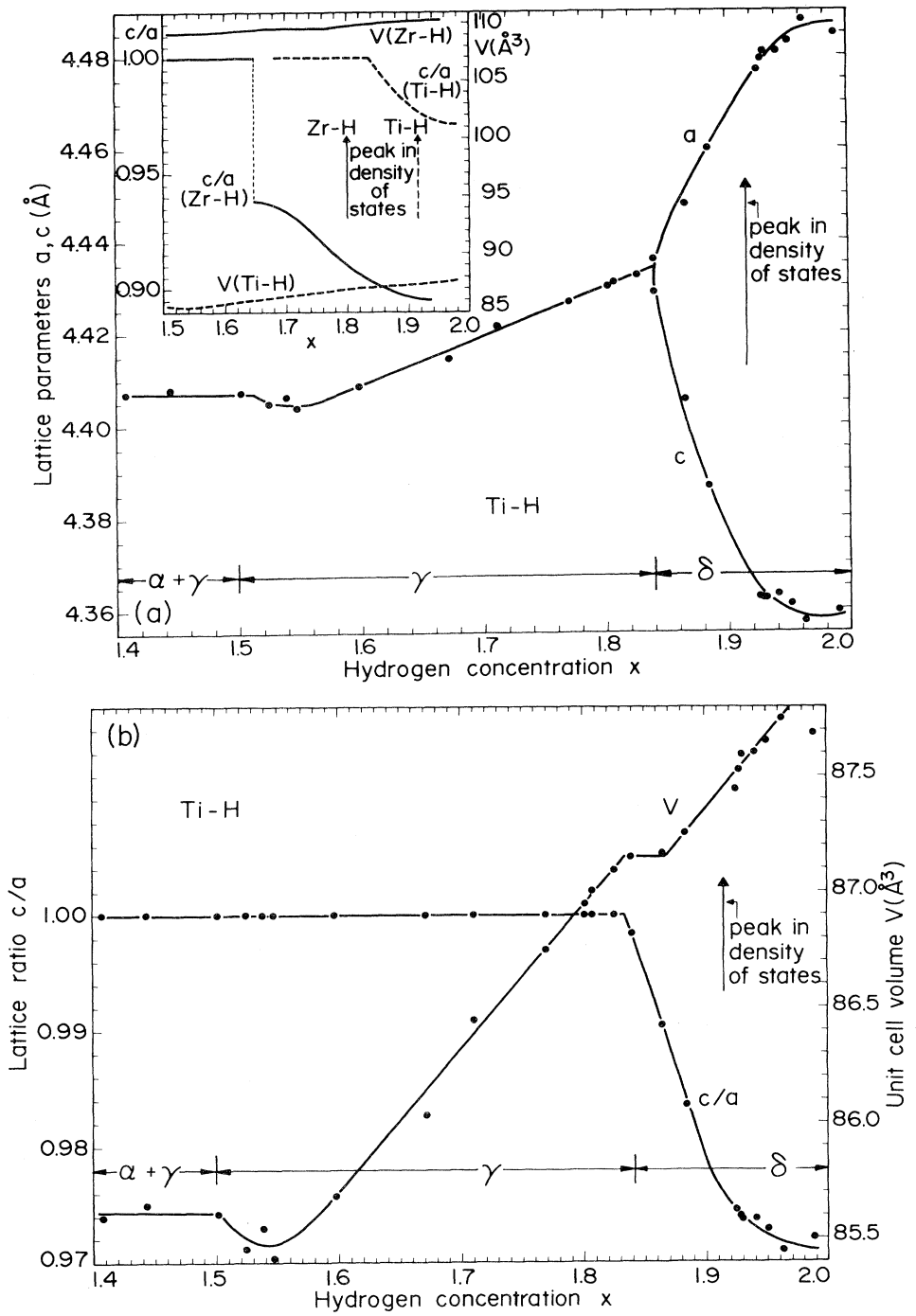

FIG. 2. Room-temperature lattice parameters of the Ti-H system showing the fcc γ phase, the fct δ phase, and the mixed $\alpha+\gamma$ region. Arrows indicate concentration at which the peak in the DOS appears as inferred from NMR. (a) Hydrogen concentration dependence of a and c, and (b) hydrogen concentration dependence of c/a and unit-cell volume V. These are compared for Zr-H and Ti-H on the same scale in the inset of (a).

a corresponding $\alpha+\delta$ region. While this is true for Ti-H, an additional metastable tetragonally distorted fct structure with $c/a > 1$ is found in this region for Zr-H and it is called the γ phase.

In the calculations of the lattice parameters for the tetragonal regions, a and c were free parameters in the least-squares-fitting analysis so that c/a in the figures represent experimental points. In regions

where it was obvious that we were in the cubic phase (e.g., no splitting of the lines), the analysis was carried out with c set equal to a in order to improve the accuracy of the calculation. All samples in the mixed-phase region ($x < 1.5$) showed traces of α hcp metal. The increase of a with hydrogen concentration in the cubic δ phase of Zr-H is not evident from the scale used in Fig. 1(a) but is discernable from the increase of V shown in Fig. 1(b). All Zr-H samples with $x < 1.5$ showed traces of the metastable γ phase with $c/a > 1$ but the percentage of the phase present was not determined.

Despite the inclusion of a mixed $\delta+\epsilon$ region for Zr-H near $x=1.65$ by some investigators, it is believed that for samples uncontaminated by oxygen, the region is vanishingly small[27] and should not be delineated in an equilibrium phase diagram.[28] Our x-ray results did not show such a mixed-phase region, and neither did our T_1 measurements, which gave a single relaxation rate. It is interesting that although there is a steady increase in volume with hydrogen concentration, when the tetragonal region is reached the volume remains constant over a small increase in x and then continues its upward climb. This plateau is more pronounced in Zr-H.

The fct γ phase of Zr-H is considered to be the stoichiometric compound ZrH as determined from neutron-diffraction studies of Sidhu *et al.*[29] Our results hint at a slight increase in c/a and V for γ occurring at higher x, which may indicate small changes from stoichiometry.

The inset of Fig. 2(a) using a single scale has been included for easy comparison of the Zr-H and Ti-H systems. It is seen that (1) although the unit-cell volume of zirconium hydride is larger than that of titanium hydride, the volume of the latter expands almost twice as much as the former upon the addition of hydrogen from $x=1.5$ to 2 ($\Delta V \approx 1.3$ Å^3 for Zr-H, $\Delta V \approx 2.3$ Å^3 for Ti-H, thus Zr-H expands by 1.2% while Ti-H expands by 2.7%), (2) the tetragonal distortion is much more severe for Zr-H than for Ti-H, and (3) the distortion for Zr-H occurs at lower hydrogen concentrations than for Ti-H.

We note for later discussion that the peak in the density of states as determined from our measurements occurs for both metals at concentrations above that where the tetragonal distortion starts.

B. Knight shift

The proton Knight shift of ZrH_x and TiH_x was measured at 295 K as a function of hydrogen concentration at a resonance frequency of 50 MHz with the use of the procedure previously described. The results shown in Figs. 3 and 4 are the averages of six measurements, the standard deviations indicated by error lines. No corrections were made for the magnetic susceptibility. This contribution, estimated from χ (Ref 20) is expected to be less than our experimental error.

The negative Ti-H Knight shift shown in Fig. 4 increases in magnitude with concentration above $x=1.5$. The curve generally follows the shape of $(T_{1e}T)^{-1/2}$ (which will be shown later in Fig. 10) for this temperature. Below $x=1.5$ we are in the $\alpha+\gamma$ region and simply observing $TiH_{1.5}$ along the entire concentration range, giving the flat result.

The Knight shift for Zr-H is also negative but smaller in magnitude than that of Ti-H. The large errors frustrate our ability to obtain the detailed shape of the concentration dependence of K other than that $|K|$ increases with x and has a maximum at the higher concentration range. K's for $x < 1.5$ are not simply those of $ZrH_{1.5}$ but are perturbed by the presence of unknown amounts of the γ phase. In both cases $|K|$ is larger for the unannealed (arrow) sample at $x=2$.

C. Concentration dependence of T_1

The proton spin-lattice relaxation time T_1 of ZrH_x and TiH_x was measured as a function of hy-

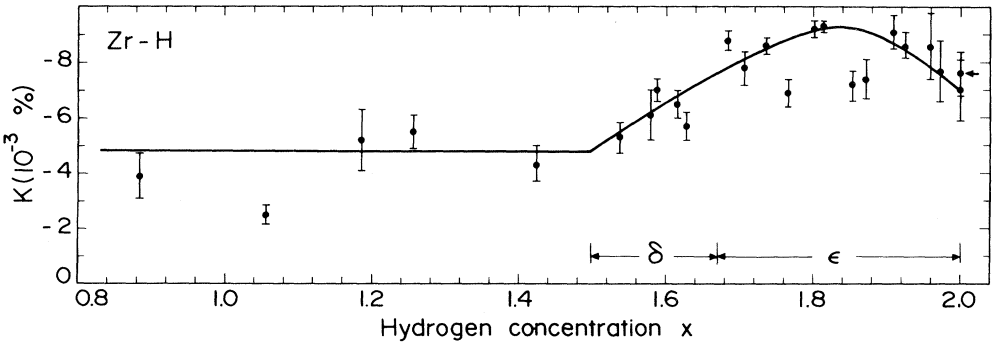

FIG. 3. Hydrogen concentration dependence of the proton Knight shift in Zr-H measured at $T=295$ K. Arrow points to the unannealed sample. Curve is drawn as a visual aid.

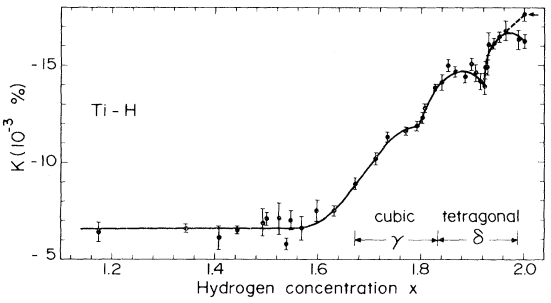

FIG. 4. Hydrogen-concentration dependence of the proton Knight shift in Ti-H measured at $T=295$ K. Arrow points to the unannealed sample. Curve is drawn as a visual aid.

drogen concentration at three different temperatures: 150, 259, and 301.5 K for ZrH_x and 150, 200, and 297 K for TiH_x. All measurements were conducted at 50 MHz except for the one at 200 K which was performed at 19 MHz. This has no significance and was due to the unavailability of a 50-MHz probe at the time of measurement. At 200 K, there is virtually no contribution to relaxation due to diffusion so that our conclusions are unaffected by this change of frequency. The results of the measurements are shown in Figs. 5 and 6.

The constancy of T_1 in the region $x<1.5$ for Ti-H is again due to the fact that only $TiH_{1.5}$ is being observed by the measurements. This is not so for the case Zr-H. Here in the region $x<1.5$, T_1 is seen to decrease significantly from its value for $ZrH_{1.5}$. This is due to the contribution of hydrogen in the γ phase. Indeed in the measurements of T_1 for $x<1.5$, a slightly nonexponential decay in the magnetization was found, indicating signals from more than one phase. Attempts were made to fit the signal amplitude to the function

$$V=V_0+M_\delta\exp(-t/T_{1\delta})+M_\gamma\exp(-t/T_{1\gamma}),$$

where t is the time between pulses, $T_{1\gamma}$ and $T_{1\delta}$ are the relaxation times for the two phases, and $M_\gamma/(M_\delta+M_\gamma)$ is representative of the fraction of hydrogen in the γ phase. This analysis was performed on the 150- and 259-K runs. The scatter resulting from this five-parameter fit was too great to yield any information about the γ phase. Hence a four-parameter fit was performed with $T_{1\delta}$ chosen to be equal to its values measured at $ZrH_{1.54}$. The results are shown in Table I. Since the γ phase is expected to be practically stoichiometric ZrH, we should obtain a single value for $T_{1\gamma}$. The scatter is too large to give an accurate value for this parameter, but it is certainly less than $T_{1\delta}$. The results indicate that in the $\alpha+\gamma+\delta$ region, $T_{1\gamma}$ is about $\frac{1}{2}$ that of $T_{1\delta}$. The points plotted in Fig. 5 were obtained from a least-squares fit of the signal-recovery data to a single exponential function. Hence the drop in T_1 in the $\alpha+\gamma+\delta$ region simply reflects the lower T_1 contribution of γ-phase ZrH.

D. Temperature and frequency dependence of T_1T

We will be interested in the parameter T_1T in order to gain information on the density of states at

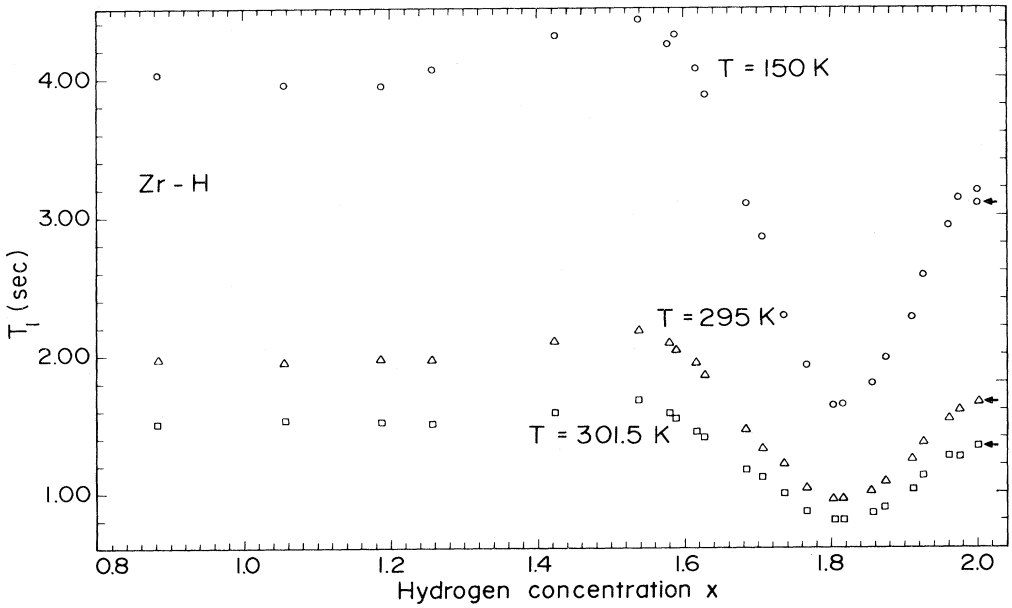

FIG. 5. Proton spin-lattice relaxation time T_1 of zirconium hydride as a function of hydrogen concentration for three different temperatures. Arrow points to the unannealed sample. Values for $x<1.5$ represent an average of two T_1's for the mixed $\gamma+\delta$ phase.

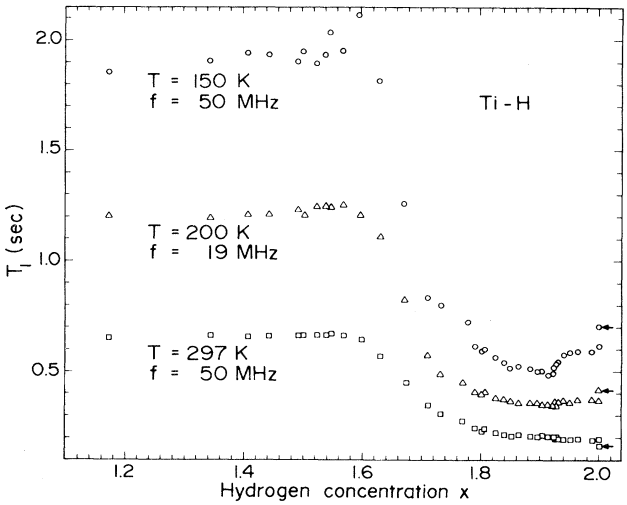

FIG. 6. Proton spin-lattice relaxation time T_1 of titanium hydride as a function of hydrogen concentration for three different temperatures. Arrow points to the unannealed sample.

the Fermi level. Data on this parameter for Ti-H was given in Ref. 2. Figure 7 shows the results obtained in this study for a number of samples of Zr-H. The curves drawn through the points are not theoretical but simply visual aids. The figure is broken up into two parts for the sake of clarity, the left-hand side giving the results for $x < 1.815$ while the right-hand side is concerned with $x > 1.815$. It is seen that contrary to expectations from elementary considerations, T_1T is not independent of temperature, but this dependence increases as we depart from $x=1.81$ on either side. Doolan *et al.*[12] also found a decrease of T_1T with temperature. While T_1T decreases with T for most of the temperature range, there is a droop in this parameter at the lower extremity.

To check on the origin of this behavior the measurements were repeated at a lower frequency for two of the samples. The samples chosen were the extreme: $ZrH_{1.81}$ which has the smallest temperature dependence of T_1T and $ZrH_{1.58}$ for which the dependence is greatest. The largest practical change in frequency was used, namely $f=16.7$ MHz and the results are shown in Fig. 8. Since any diffusional relaxation contributor goes as f^2 on the low-temperature side, any such contribution in our case would be magnified ninefold. Similarly paramagnetic relaxation contributions may be frequency dependent.

Figure 8 shows that the frequency dependence is greatest in the drooping low-temperature region of the curve with only a small effect in the intermediate region. The sudden drop of T_1 on the high-temperature side is simply due to hydrogen diffusion, the effect of which disappears exponentially as the temperature is lowered. We will concern ourselves only with data at temperatures below this cutoff. The diffusional contribution is indeed seen to become effective at lower temperatures for the lower frequency.

IV. DISCUSSION

A. NMR interactions

The relation describing the NMR relaxation rate due to the conduction electrons in transition metals is given by[30]

$$(T_{1e}T)_0^{-1}=4\pi\gamma_n^2\hbar k_B\{[H_{\rm hf}^{(s)}N_s(E_F)]^2+[H_{\rm hf}^{(d)}N_d(E_F)]^2q+[H_{\rm hf}^{(o)}N_d(E_F)]^2p\}\ , \quad (1)$$

where $H_{\rm hf}^{s,d,o}$ are the hyperfine-field contributions at the nucleus due to s-contact interaction, d-electron core polarization, and d-electron orbital interaction, p and q are reduction factors, and N_s and N_d are the s- and d-electron contributions to the density of states for one direction of spin at the Fermi level. The 0 subscript on $(T_{1e}T)$ will be clarified later.

TABLE I. Result of two exponential-decay analyses for finding T_1 in the γ phase of ZrH.

x	$M_\gamma/(M_\gamma+M_\delta)$	$T_{1\gamma}$ (sec)	
1.42	0.04	0.7	$T=259$ K
1.26	0.17	1.3	$T_{1\delta}$ set equal to 2.17 sec
1.19	0.24	1.4	
1.05	0.15	0.9	
0.885	0.14	1.0	
1.42	0.03	1.4	$T=150$ K
1.26	0.10	1.7	$T_{1\delta}$ set equal to 4.41 sec
1.19	0.15	2.0	
1.05			
0.885	0.11	1.7	

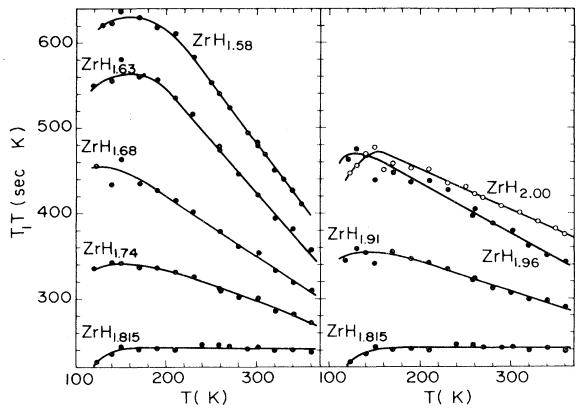

FIG. 7. Temperature dependence of T_1T in ZrH_x for $x<1.81$ (left-hand side) and $x>1.81$ (right-hand side). Curves are drawn as visual aids.

$N_s(E_F)$ can be neglected with respect to $N_d(E_F)$ in transition metals (where E_F lies in the d band), and this is born out in our case by the negative Knight shift for which the s-electron contribution is positive and by the calculations of Gupta for TiH_2.[7] Hence (1) reduces to the form

$$(T_{1e}T)_0^{-1/2}=AN_d(E_F)\ , \tag{2}$$

and $(T_1T)_0^{-1/2}$ is a measure of the density of states at the Fermi level. For reasons to be discussed later, the dominant hyperfine interaction is probably core polarization and we write

$$A^2=4\pi\gamma_n^2\hbar k_B[H_{\rm hf}^{(d)}]^2q\ . \tag{3}$$

Figures 9 and 10 show the variation of $(T_1T)^{-1/2}$ with hydrogen concentration for ZrH_x and TiH_x.

B. Zr-H system

1. Concentration dependence

Consider first the ZrH_x system. $(T_1T)^{-1/2}$ first increases and then decreases with x with the peak occurring at $x=1.80$ (Fig. 9) By varying the hydrogen concentration we vary the number of electrons in the conduction band. Switendick's calculations[31] indicate that between about 0.4 to 1.0 electrons per hydrogen atom are removed from the conduction band when lowering the concentration from its stoichoimetric composition TiH_2. Assuming that changing x within the nonstoichiometric region

$$(T_{1e}T)^{-1}=(T_{1e}T)_0^{-1}\left[1+\tfrac{1}{3}\pi^2k_B^2\left[\frac{1}{N(E)}\frac{d^2N(E)}{dE^2}\right]_{E=E_F}T^2\right]\ , \tag{4}$$

where $(T_{1e}T)_0$ is the value of $T_{1e}T$ when $T\to0$ K. The temperature dependence due to this effect is usually negligible since it involves the second derivative.

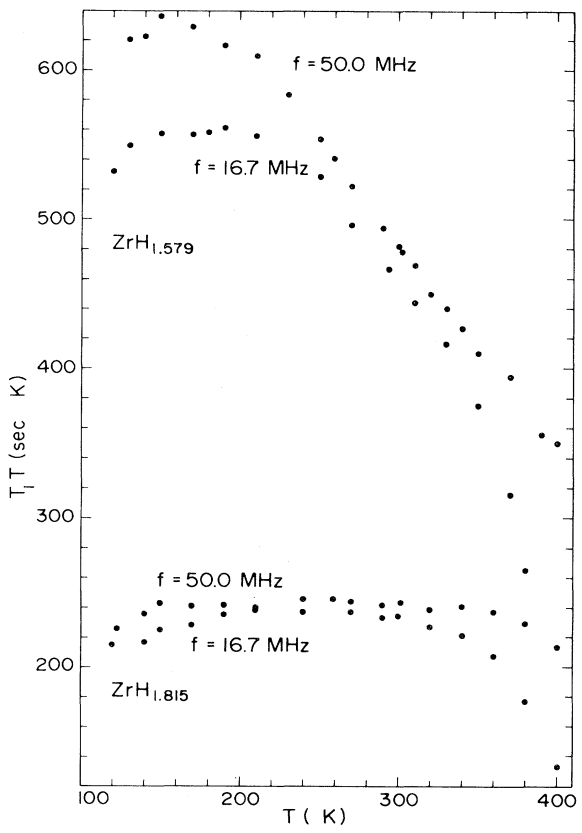

FIG. 8. Effect of resonance frequency on temperature dependence of T_1T for $ZrH_{1.579}$ and $ZrH_{1.815}$.

$1.5<x<2.0$ has only a minor effect on the density of states, varying the hydrogen concentration across this range effectively sweeps the Fermi level across a portion of the density-of-states curve and $(T_1T)^{-1/2}$ reflects its structure. Comparison with the theoretical curve for cubic ZrH_2 obtained by Gupta[18] will be made later.

2. Effect of temperature

Equation (1) implies that T_1T should be temperature independent and thus the individual curves for the three different temperatures in Figs. 9 and 10 should coincide. The derivation of Eq. (1) depends, however, on the assumption of an infinitely sharp Fermi-distribution step function, i.e., $T\to0$ K. At finite temperatures one obtains[32]

The temperature dependence of T_1T was investigated for a number of samples. In order to ascertain whether this dependence is a property of some special peculiarity at certain hydrogen concentrations,

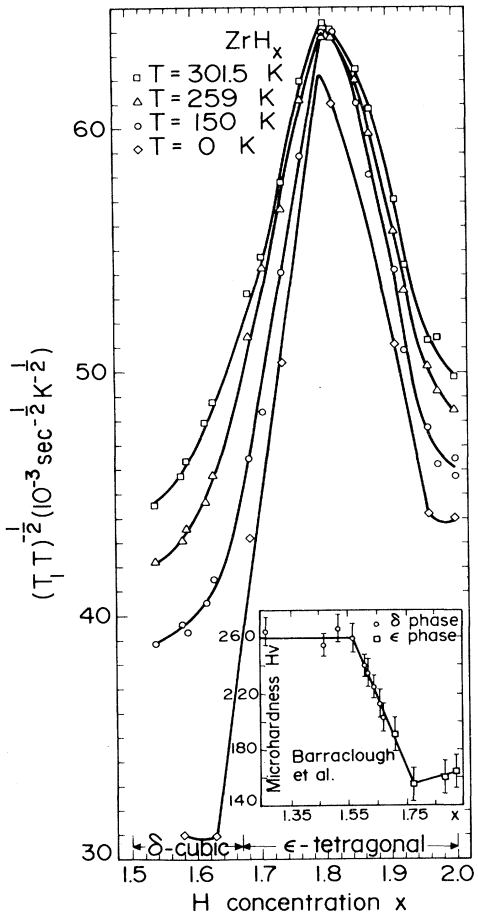

FIG. 9. Concentration dependence of $(T_1T)^{-1/2}$, a measure of the DOS at the Fermi level for Zr-H at $T=301.5$, 259, 150, and 0 K. Extrapolation method for the last result is explained later in text. Inset: concentration dependence of microhardness for the Zr-H system after Barraclough *et al.* (Ref. 27).

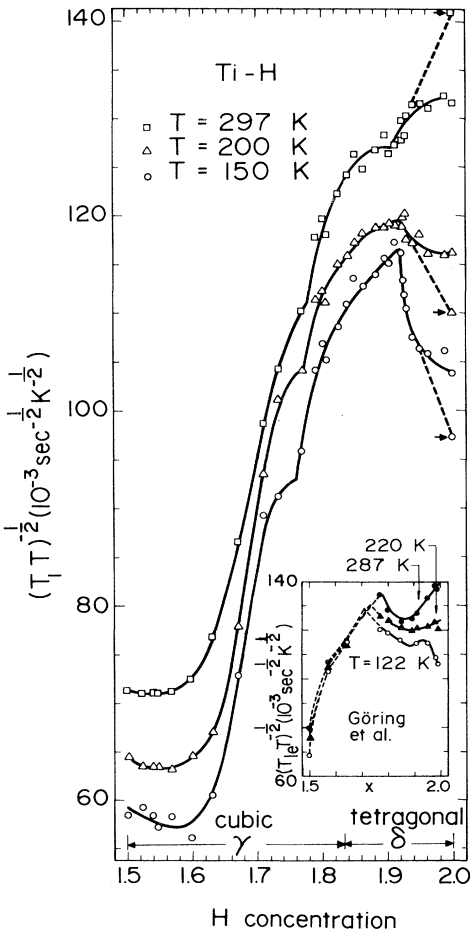

FIG. 10. Concentration dependence of $(T_1)T^{-1/2}$, a measure of the DOS at the Fermi level for Ti-H at $T=297$, 200, and 150 K. Arrows point to unannealed sample. Inset: results of Goring *et al.* (Ref. 4).

the following hydrides were chosen: $ZrH_{1.58}$, $ZrH_{2.00}$ (annealed), $ZrH_{1.815}$, $ZrH_{1.63}$, $ZrH_{1.68}$, $ZrH_{1.74}$, $ZrH_{1.91}$, and $ZrH_{1.96}$. The first and second are near the lowest- and highest-concentration samples available in the hydride range. The third is near the peak of $(T_1T)^{-1/2}$. The fourth and fifth have adjacent concentrations but are on opposite sides of the tetragonal deformation. The sixth and seventh have nearly the same $(T_1T)^{-1/2}$ but the former lies on the rising slope of the $(T_1T)^{-1/2}$-vs-x curve, while the latter is on the falling side. The last sample was added for good measure. The results show (Fig. 7) that the changes of T_1T with temperature cannot be correlated with any of these events. The only trend we see is that near the peak of $(T_1T)^{-1/2}$, T_1T is nearly temperature independent and the decrease of T_1T with temperature becomes stronger when the concentration moves away from this peak on either side. We conclude, therefore, that the temperature dependence is primarily connected with the shape of the density of states, following Eq. (4). Although this dependence should ordinarily be very small, in our case we are in a region of a very sharp peak in the density of states as our measurements and the calculations of Gupta[18] show. We thus attempt to fit our data to the function

$$(T_{1e}T)^{-1}=C+MT^2\,. \tag{5}$$

In order to do this we must obtain T_{1e} from T_1. Relaxation due to hydrogen diffusion can be neglected in this temperature range. Since $(T_{1e})^{-1}\propto T$, at low enough temperatures the relaxation contribution due to this process becomes small enough that relaxation due to paramagnetic centers becomes significant. We can see from the rounding off and dropping of T_1T below about 180 K (Fig. 7) and the greater frequency dependence of T_1T in this low-

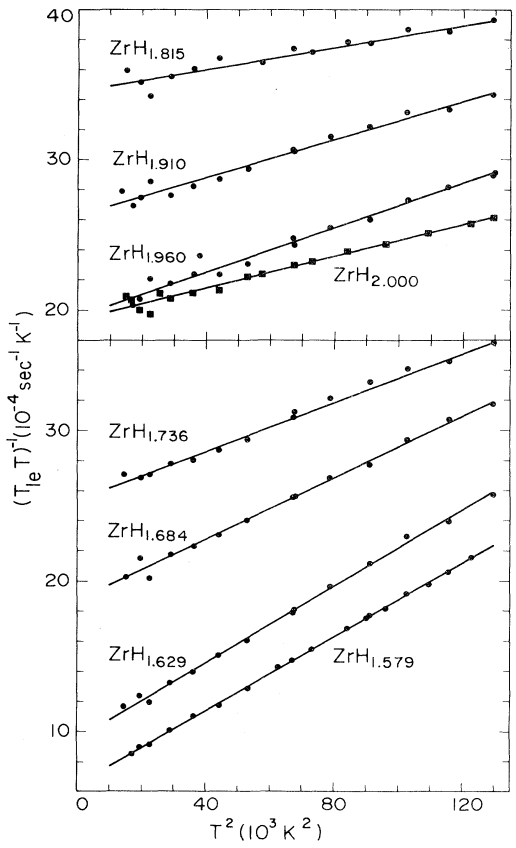

FIG. 11. $(T_{1e}T)^{-1}$ of Zr-H as a function of T^2 showing Eq. (4) is satisfied. Theoretical lines and T_{1e} were obtained using the values of M, C, and T_{1p}^{-1} derived from a least-squares fit.

temperature region (Fig. 8) that paramagnetic contributions are having some effect on our measurements. While T_{1e} should be resonance frequency independent, the relaxation contribution due to

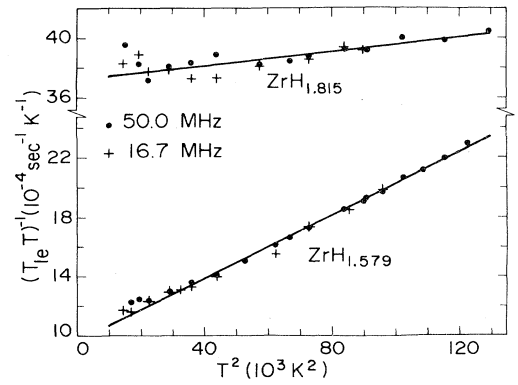

FIG. 12. Reduction of data of Fig. 8 for two frequencies into a single $(T_{1e}T)^{-1}$-vs-T^2 relation under the assumption $T_{1p}^{-1} \propto f^{1/2}$ in the region where relaxation due to diffusion can be ignored.

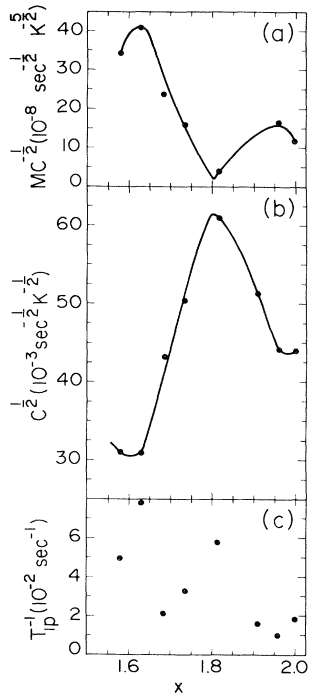

FIG. 13. Plots of parameters obtained from a least-squares-fit analysis of the temperature and frequency dependence of T_1T in ZrH_x. (a) $MC^{-1/2}$ is proportional to $[d^2N(E_F)/d^2E]_{E=E_F}$, (b) $C^{1/2}$ is proportional to $N(E_F)$, and (c) shows paramagnetic contributions to the relaxation rate.

paramagnetic impurities, T_{1p}^{-1}, should have an $f^{1/2}$ dependence[33] (as we shall soon see is indeed the case here) and be practically temperature independent.

Zogal and Idziak[34] attempted to extract the paramagnetic contribution to the relaxation rate in Sc-H by assuming it to be constant and fitting the data to

$$(T_1T)^{-1}=A+(T_{1p}T)^{-1} .$$

Our results do not follow this relation. We must invoke the T^2 dependence. Wiley *et al.*[35] and Goring *et al.*[4] found T_{1p}^{-1} in Pd-H and Ti-H, respectively, by extrapolating T_1^{-1} vs T through low-temperature data ($\sim$4K) to 0 K so that the ordinate intercept gives T_{1p}^{-1}. Since the lowest temperature in this study was $\sim$120 K, this method is inapplicable here. Instead a least-squares fit to (5) was taken with the use of

$$T_1^{-1}=T_{1e}^{-1}+T_{1p}^{-1} , \tag{6}$$

$$(T_1T)^{-1}=C+MT^2+(T_{1p}T)^{-1} , \tag{7}$$

where

$$C=(T_{1e}T)_0^{-1} , \tag{8}$$

$$M=\tfrac{1}{3}\pi^2 k_B^2 (T_{1e}T)_0^{-1}\left[\frac{1}{N(E)}\frac{d^2N}{dE^2}\right]_{E=E_F}, \quad (9)$$

and the free parameters were C, M, and T_{1p}^{-1}. The results are shown in Fig. 11 and indicate that the data satisfy Eq. (5). The straight lines in the figure are the fits to Eq. (5) using the calculated M's, C's, and T_{1p}^{-1}'s.

A further indication that our low-temperature results are affected by paramagnetic impurities is obtained from the data of Fig. 8. T_{1e} should be frequency independent. It is seen that in the lower-temperature region the low-frequency $(T_1T)^{-1}$ droops more strongly than the high-frequency one. This is expected if the droop is indeed due to paramagnetic impurity relaxation whose strength goes as $f^{-1/2}$.[33] Thus the equality T_{1p}^{-1} (at 16.7 MHz)/T_{1p}^{-1} (at 50 MHz)$=(50/16.7)^{1/2}=1.7$ should hold. When a least-squares analysis of the low-frequency data was performed for the samples $ZrH_{1.58}$ and $ZrH_{1.815}$ the resulting T_{1p}^{-1} (at 16.7 MHz)/T_{1p}^{-1} (at 50 MHz) ratios were 1.3 and 1.9, respectively, or on the average 1.6. Since the measurements were performed in a region where T_{1e} dominates, better agreement should not be expected. The analysis was repeated with the use of the same number of free variables as previously, namely C, M, and T_{1p}^{-1} but this time with the use of the combined data at the two frequencies with the restriction T_{1p}^{-1} (16.7 MHz)$=1.7T_{1p}^{-1}$ (50 MHz). The results are shown graphically in Fig. 12. These M, C, and T_{1p}^{-1} are considered the more accurate ones since the low-frequency data emphasized T_{1p}^{-1} while those at high frequency did so for M and C (in which we are primarily interested). Figure 13 employed these values. Figure 12 shows that when the influence of T_{1p}^{-1} is included with a frequency dependence of $f^{-1/2}$, the data of T_{1e} result in a single universal $(T_{1e}T)^{-1}$ curve for both frequencies.

Equations (2), (8), and (9) imply that

$$\sqrt{C}=(T_{1e}T)_0^{-1/2}=AN_d(E_F) \quad (10)$$

and

$$\frac{M}{\sqrt{C}}=(\tfrac{1}{3}\pi^2 k_B^2 A)\left[\frac{d^2N_d}{dE^2}\right]_{E=E_F}. \quad (11)$$

Thus $\sqrt{C}$ and $M/\sqrt{C}$ are proportional to the density of states and the second derivative of the density of states at the Fermi level. The results of the least-squares analysis are plotted in Fig. 13. They indicate a cuspidal shape for $N_d(E)$ vs E. Near the peak of the density of states (at $x=1.8$), $d^2N(E)/dE^2$ is very small showing a linear variation of $N_d(E)$. As one moves away to either side of this peak, d^2N/dE^2 increases, i.e., the curvature of $N_d(E)$ increases. At the ends of the peak where $N_d(E)$ levels out, the curvature is a maximum as would be expected. It should be noted that the density-of-states curve and the d^2N/dE^2 results confirming this shape are derived from independent measurements. The general shape can be ascertained from the concentration dependence of T_1 obtained at low temperature, as indicated in Fig. 9, while d^2N/dE^2 is gotten from the temperature dependence of the NMR parameters.

While the symmetric trend of the thermal behavior about $x=1.80$ and the satisfactory fit to the theoretical equation indicates that the primary cause of the temperature dependence is that just described, there is probably also a contribution from direct changes in the electronic structure caused by thermal expansion and the temperature dependence of the degree of tetragonality. These effects would influence the accuracy of the parameters shown in Fig. 13.

Figure 13(c) shows that there is no trend in T_{1p}^{-1} as far as hydrogen concentration is concerned so that one cannot extrapolate these values to estimate their contribution to those samples where the temperature dependence of T_1 was not measured. Since these contributions make only minor adjustments to T_{1e}, we leave Fig. 9 as is, plotting $(T_1T)^{-1/2}$ instead of $(T_{1e}T)^{-1/2}$. Nevertheless, the figure gives a good overall indication of $N(E_F)$.

Although of relatively small influence at the temperatures employed in this study, T_{1p} would completely dominate the relaxation in the mK range in the ZrH_2 measurements of Zweers *et al.*[10] Their T_1T, which they ascribed to relaxation due to conduction electrons, is almost an order of magnitude smaller than reported here. Attributing the relaxation to paramagnetic impurities would explain the large field dependence they obtain for T_1 which they estimate to go as f^3 and would correspond to the rapid spin-diffusion case.[33] T_1T obtained in this study agree with the results of Pope *et al.*[13] when extrapolated to 500 K.

3. *The reduction factor q*

Since a Korringa-type relation exists for core polarization, q in Eqs. (1) and (3) may be obtained from[32]

$$K^2T_{1e}T=\left[\frac{4\pi}{h}\left[\frac{\gamma_p}{\gamma_e}\right]k_Bq\right]^{-1}, \quad (12)$$

where γ_e and γ_p are the gyromagnetic ratio of an electron and proton. The q we obtain for Zr-H by comparing the room-temperature K with $T_{1e}T$ has very large scatter, reflecting the large scatter in K.

No hydrogen concentration dependence was discerned within the experimental error, thus the average and mean-square deviation was taken for the q at different x, giving

$$q = 0.13 \pm 0.03 \ .$$

This parameter will be discussed more fully in conjunction with Ti-H.

4. *Connection with the density of states*

While our results yield information on the relative values of the density of states for different hydrogen compositions, it would be useful to have some estimate of absolute values. The parameter $\sqrt{C} = (T_{1e}T)^{-1/2}$ which we obtain from our measurements is proportional to the density of states at the Fermi level with the proportionality constant A defined in Eq. (10). To obtain A we compare our results with the density of states obtained by Ducastelle *et al.*[21] from their low-temperature heat-capacity measurements. They found $N(E_F)$ to be equal to 0.36, 0.76, and 0.46 states/eV for one direction of spin for $ZrH_{1.55}$, $ZrH_{1.85}$, and $ZrH_{1.96}$, respectively, while our corresponding values of $\sqrt{C}$ are 0.032, and 0.059, and 0.044 $(\sec \mathrm{K})^{-1/2}$. This yields $A = 0.089$, 0.078, and 0.096 $\mathrm{eV}\,(\sec \mathrm{K})^{-1/2}$. The almost constant value of A shows satisfactory agreement especially since $N(E_F)$ and $\sqrt{C}$ vary sharply so that small differences in hydrogen concentration between the two studies would yield a large error. The results also indicate that q, which is related to A by Eq. (3), is practically constant over the whole concentration range. The average value of A is 0.087 $\mathrm{eV}/(\sec \mathrm{K})^{1/2}$. Ducastelle *et al.* did not take into account the phonon interaction parameter λ which Bohmhammel *et al.*[22] show should be approximately 0.3 for the hydrides. Multiplying by $(1 + 0.3)$ we obtain

$$A = 0.11 \ ,$$

in units of $\mathrm{eV}/(\sec \mathrm{K})^{1/2}$. If we substitute this value of A into Eqs. (10) and (11) we find that dividing the ordinate in Fig. 13(b) by 0.11 gives the density of states in number of states for one direction of spin/eV/atom and multiplying the ordinate of Fig. 13(a) by 3.7×10^8 [Eq. (11)] gives $(d^2N/dE^2)_{E_F}$ in states/$(\mathrm{eV})^3$. Equation (3) and the above value of q and A gives us a hyperfine field of

$$H_{\mathrm{hf}}^{(d)} = 13.5 \ ,$$

in kgauss.

5. *γ phase*

The measurements show that T_1 in the γ phase (Table I) is very roughly about $\frac{1}{2}$ of the T_1 of $ZrH_{1.5}$ with which it coexists. Since this holds true at both 150 and 259 K, we cannot attribute this stronger relaxation to a diffusional component but it is probably due to a stronger conduction-electron contribution. The average value of $T_1\gamma$ at $T = 259$ K is 1.06 sec and that at 150 K is 1.70 sec. Thus T_1(at 150 K)/T_1 (at 259 K) $= 1.6$ while the ratio of the two temperatures is $259/150 = 1.7$, indicating that $T_1T \approx$ const holds. Sidhu *et al.*[29] have shown the composition of the γ phase to be ZrH. If we scan the TiH_2 density-of-states diagrams of Switendick[14] and Gupta[17] we find that the density of states strongly decreases at lower energies where we might expect the Fermi energy to be for this composition. It is thus likely that a completely different electronic structure exists for the hydride. This is born out by its much larger cell volume and tetragonality when compared to the host hydride.

C. Ti-H system

While the conditions that influenced $(T_1T)^{-1/2}$ for the case of ZrH_x (such as the thermal dependence and paramagnetic contribution) also probably hold for TiH_x, no comparable temperature and frequency dependence measurements were performed on the latter hydride. Nevertheless, as was seen for ZrH_x, the $(T_1T)^{-1/2}$ results should be sufficient to give a good overall picture of the electronic structure. Some temperature dependence data are given in Ref. 2 and will be referred to here.

Comparison of Fig. 10 with Fig. 9 shows that the behavior of $(T_1T)^{-1/2}$ is somewhat different for TiH_x Than ZrH_x. In Ref. 2 only a very limited number of samples were measured and curves were drawn through the experimental points which approximated the shapes of susceptibility curves.[20] Although the values in the two studies are in agreement, the present results do not justify the extrapolations made in Ref. 2. We note that the room-temperature $(T_1T)^{-1/2}$ and K (Fig. 4) follow the same pattern. While the susceptibility results of Trzebiatowsky *et al.*[20] show a peak at $x = 1.8$ (near the concentration where the tetragonal deformation takes place), $(T_1T)^{-1/2}$ goes through a smooth rise. At $x = 1.9$, χ goes through a trough while $(T_1T)^{-1/2}$ has a peak with a sharp break (at lower temperatures). At $x = 2$, χ rises again while $(T_1T)^{-1/2}$ goes down. Thus the NMR results differ in shape from those obtained for susceptibility measurements. The shape of χ was confirmed by Nagel *et al.*[36] My NMR results are, however, in agreement with the low-temperature specific-heat measurements of Bohmhammel *et al.*[22] who also obtained a single maximum of γ (proportional to the density of states at the Fermi level) at $x = 1.9$ instead of a trough. To compound the mystery both $(T_1T)^{-1/2}$ and K of

Goring *et al.*[4] show a pattern similar to that of χ at moderately low temperatures. Below 120 K, Goring *et al.* also see a peak in $(T_1T)^{-1/2}$ and K at $x=1.9$, but the peak at $x=1.8$ remains (inset of Fig. 10).

In an attempt to explain the discrepancy between my results and those of Goring *et al.*, I considered the following. Say that in the sample preparation I had mixed the pure Ti not with TiH_2 but with a lower concentration so that all the concentration values are shifted down by 0.1. This would put the peak in the same place as Goring's and the drop in $(T_1T)^{-1/2}$ seen here would be the beginning of the trough which would not rise again since our maximum concentration would be $x=1.9$. This was discounted for the following reasons: (1) It would not explain the absence of a trough at 297 K which Goring *et al.* and Trzebiatowsky *et al.* obtain at this temperature, (2) the concentration-dependent x-ray results are in agreement with the room-temperature results of Azarkh *et al.*,[24] (3) while the peaks of χ and $(T_1T)^{-1/2}$ of Goring *et al.* coincide with the concentration heralding the onset of the tetragonal phase, the peak here is located above this concentration [my x-ray and $(T_1T)^{-1/2}$ measurements were performed on the same samples], (4) the results here agree with those of Bohmhammel *et al.*, and (5) Goring *et al.* also see a peak at $x=1.9$ developing in K and $(T_1T)^{-1/2}$ at low enough temperatures while χ of Trzebiatowsky *et al.* do not.

The only manner by which I can explain the difference in the results is connected with sample-preparation techniques. The samples used here were annealed for an extended period in their sealed ampoules. Azarkh *et al.*[24] found that they were able to retain the cubic phase over the entire concentration range, the tetragonal distortion occurring only for those samples that had undergone prolonged annealing. Bohmhammel *et al.* (with whom the results here agree) also stressed the importance of the role of homogenization where they stated that the heat capacity and susceptibility were different for samples where these precautions were not taken. Differences in $(T_1T)^{-1/2}$ for TiH_2 for the annealed and unannealed samples were also found in this study, as indicated in Fig. 10. Possible effects of annealing on the long-range order of the direction of the c axis were discussed in Ref. 2 and this may have an influence on the behavior of χ and $(T_1T)^{-1/2}$. Strong annealing effects were also observed in the Ti-Al-H system.[37]

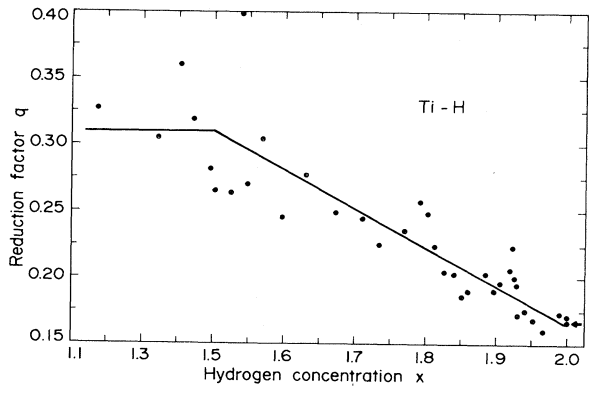

FIG. 14. Hydrogen-concentration dependence of the reduction factor q for TiH_x at $T=297$ K.

In Ref. 2 the hyperfine interaction was attributed to orbital interactions. This was based on a comparison between the measured hydrogen concentration dependence of $(T_1T)^{-1/2}$ and K obtained by Stalinski *et al.*[7] The shape of the two should differ if the interaction is mostly orbital and be similar for core polarization. Since they differed, an orbital interaction was assumed. The Knight-shift results obtained here do not agree with those of Stalinski *et al.*; nor do those of Frisch *et al.*[8] and Goring *et al.*[4] Comparing Figs. 4 and the room-temperature result of Fig. 10, we see that the two are of the same shape. Goring *et al.* also obtained similar shapes for $(T_1T)^{-1/2}$ and K. Thus it is concluded that the negative shifts and relaxation mechanisms are due to core polarization. Similar conclusions were drawn by Goring *et al.*,[4] Bowman *et al.*,[5] and Nowak *et al.*[6] We can thus obtain q from Eq. (12), and the result for $T=297$ K is plotted in Fig. 14. q decreases steadily from 0.31 to 0.165 as x ranges from 1.5 to 2.0. Goring *et al.* found a similar decrease of q with hydrogen concentration but there the range was 0.54 to 0.22. The special methods employed by Goring *et al.* in their determination of K (multiple pulse sequence with magic angle spinning) both narrowed their lines (which in this study is many times wider than the resonance shift) and automatically eliminated susceptibility effects which may account for the difference between the two results.

Goring *et al.* (as well as Nowak *et al.*[6] and Korn[2]) analyzed their data in terms of the cubic symmetry of the fcc structure of the hydride. For this case q ranges from a maximum of 0.5 to a minimum of 0.2. This occurs when the t_{2g} character at the Fermi level goes from 0 to 0.6[32] Thus Goring's results could be interpreted in accordance with the phenomenological picture presented in Ref. 2 whereby the minimum hydrogen concentration is assumed to coincide with the start of t_{2g} character, i.e., there is no t_{2g} admixture for $TiH_{1.5}$ and that more t_{2g} character comes in as x increases. Fujimori and Tsuda[19] have broken up the $3d$ density of states into their e_g and t_{2g} character. They indeed found

that below the Fermi level for TiH_2 (where we would expect the Fermi level for $TiH_{1.5}$ to be) the character is almost completely of the e_g type with strong t_{2g} admixture at the higher energy corresponding to the Fermi level for TiH_2. However, the band calculations that have been performed to date[15,17,19,38] make the validity of the broader picture presented in Ref. 2 very doubtful. The lower q values found in this study and those of Goring *et al.* could be compatible with theory if one takes into consideration that the immediate environment of the hydrogen is tetrahedral. If one considers the core polarization to be due to hydrogen centered orbitals arising from a combination of metal d electrons at the Fermi level interacting with hydrogen-centered inner-valence s electrons, then Ehrenfreund[39] showed that q can take on values that range from 0.05 to 1.

The overall shape of $(T_1T)^{-1/2}$ obtained here is consistent with density of states obtained by Bohmhammel *et al.*[22] from low-temperature specific-heat measurements. Since q varies with concentration, we must use $(T_1T)^{-1/2}/\sqrt{q}$ to get a value that is proportional to the density of states. However, q varies slowly with x and $\sqrt{q}$ ranges from 0.56 to 0.41 as x goes from 1.5 to 2, so the overall shape of Fig. 10 is only slightly effected. Since, according to Goring *et al.*, q rises somewhat for x near 2 at low temperature, the shape is even less effected. For comparison, we take the ratios $N_d(x=1.9)/N_d(x=1.55)$ and $N_d(x=1.9)/N_d(x=2.0)$ of Bohmhammel (i.e., the ratios between N_d at the peak and the two ends) and compare these to the respective ratios of $(T_1T)^{-1/2}/\sqrt{q}$. These give 2.0 and 1.2 from specific heat as compared to 2.5 and 1.2 from NMR at 150 K, which is satisfactory. In order to obtain an approximate calibration of the ordinate in Fig. 10, we define B by $A=\sqrt{q}B$ where A is that of Eq. (2). Comparing Bohmhammel's density of states with the 150-K $(T_1T)^{-1/2}$ and $\sqrt{q}$ at the peak, we obtain $B=0.30$ eV atom/sec$^{1/2}$ K$^{1/2}$, so that if the ordinate in Fig. 10 is divided by $0.30\sqrt{q}$ where $\sqrt{q}$ is obtained from Fig. 14, a rough value of the density of states at the Fermi level is obtained in units of eV^{-1} atom^{-1} for one direction of spin.

Since

$$B=2\gamma_N H_{\rm hf}^d(\pi\hbar k_B)^{1/2},$$

we obtain $H_{\rm hf}^d=13.4$ kG. This is in agreement with what we obtained for Zr-H for which we found $H_{\rm hf}^d=13.5$ kG. Thus by assuming the same hyperfine interaction for Zr-H as for Ti-H we obtain that the larger values of K and $(T_1T)^{-1/2}$ of Ti-H as compared to Zr-H [a factor of about 1.6 at the peak for the low-temperature $(T_1T)^{-1/2}/\sqrt{q}$] is due to the larger density of states of the former. This agrees with the theoretical results of Gupta[18] who also obtained a larger density of states for TiH_2 than ZrH_2 where the ratio was 1.4 at the peaks. The value Goring *et al.*[4] obtained for the hyperfine field at the proton in Ti-H was 8.3 kG while Nowak *et al.*[6] found it to be 8.8 kG in Ti-H-Nb.

D. Comparison with electronic structure: Tetragonal deformation

Since extensive band calculations have been published for cubic TiH_2 and ZrH_2, an attempt will be made to compare these with the measurements. It will be seen that a simple straightforward extension of the theory to the nonstoichiometric case cannot be made without invoking further hypotheses.

Figure 15(a) shows the density of states for cubic ZrH_2 calculated by Gupta.[18] The corresponding diagram for cubic TiH_2 is very similar except for scale.[17] A central theme in the Switendick-Gupta theory is that the Fermi level lies at the center of a peak in the density of states derived mostly from the flat doubly degenerate states joining Γ_{25}' and L_3 in the Λ direction. The tetragonal distortion is attributed to a Jahn-Teller effect which splits the degenerate states. As an aid to the discussion the result expected from such a split in schematically sketched in Fig. 15(b)

Let us see how the concentration dependence of $(T_1T)^{-1/2}$ can be understood according to this description. The results of the band splitting can be followed by comparing $(T_1T)^{-1/2}$ for TiH_x at 297

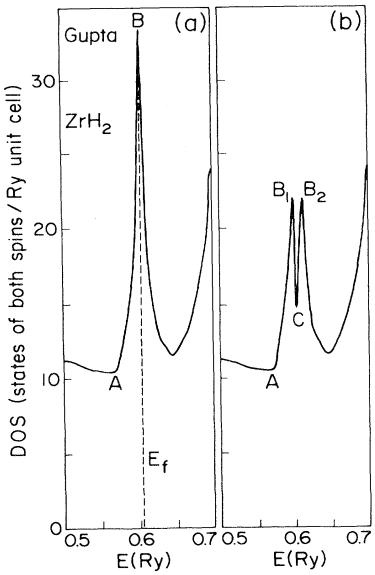

FIG. 15. (a) Gupta's (Ref. 18) DOS near the Fermi level for cubic ZrH_2, and (b) sketch of presumed DOS upon splitting of the doubly degenerate states.

K (where the tetragonal distortion is very small) with the low-temperature results for TiH_x and ZrH_x at all three temperatures (where the distortion is large). At 297 K, $(T_1T)^{-1/2}$ for TiH_x is seen in Fig. 10 to rise steadily as x ranges from 1.5 to 2 in accord with the assumption that the Fermi level moves to higher energy and thus to larger density of states with increasing x, and that the Fermi level at $x=2$ lies at the center of the peak of the density of states. At lower temperatures the tetragonality increases and so does the splitting. In particular $(T_1T)^{-1/2}$ decreases drastically in the high-x region. By observing the temperature dependence of $(T_1T)^{-1/2}$ for TiH_2 given in Ref. 2, one can follow how part of the peak breaks away as the tetragonality is increased with decreasing temperature. Since at $x=2$ only half of the degenerate band is occupied, the splitting of the band into parts above and below the Fermi level must cause the electrons to spill into the lower peak and completely fill it. Thus we can associate $(T_1T)^{-1/2}$ at $x=2$ for TiH_x at 297 K with point B of Fig. 15(a) while the low-temperature peaks of TiH_x and that of ZrH_x are associated with B_1 of Fig. 15(b) and their values at $x=2$ with point C of the same figure. Gupta's density of states at the Fermi level for cubic ZrH_2 is 1.21/eV atom for one direction of the spin which for our value of $A=0.11$ eV $\sec^{-1/2}K^{-1/2}$ gives an expected $(T_1T)^{-1/2}$ of 0.133 $\sec^{-1/2}K^{-1/2}$. This is a reasonable value when extrapolating the rising part of the $(T_1T)^{-1/2}$ curves in Fig. 9 to $x=2$. It is twice the value obtained at the peak (0.062 $\sec^{-1/2}K^{-1/2}$). Since not all the states at the Fermi level are derived from the degenerate states one would not quite expect a doubling but an exact comparison cannot be made anyway since the lattice expansion with hydrogen concentration would effect the density of states somewhat. The general trends, however, follow the outline of the experimental curves.

The problem with this description is that for both TiH_x and ZrH_x, $(T_1T)^{-1/2}$ increases continuously as x increases across the distortion. As soon as the first sample in the tetragonally distorted region is reached, there should be an abrupt discontinuity in the curve as the density-of-states configuration changes from that described in Fig. 15(a) to that in Fig. 15(b). No such sharp break is observed. One may argue that the reason a sharp break is not observed is because perhaps the Fermi level lies below the degenerate states at the concentration where the tetragonal distortion takes place. This would, however, negate the conclusion that the tetragonal deformation is caused by a Jahn-Teller interaction which requires the Fermi level to lie within the degenerate states.

I would like to speculate on a possibility that would be in accord with both the Switendick-Gupta description and the experimental results. It supposes that the degenerate states are always split. At low hydrogen concentration the vacancies spoil the symmetry, splitting the degenerate states. An example of such a possibility is illustrated by the cases of V_3Si and Nb_3Sn where calculations showed[40] that either vacancies in a cubic structure or a tetragonal distortion can split the degenerate Γ_{12} band. As x increases there are not enough vacancies to support the splitting and the Jahn-Teller effect takes over and the crystal structure becomes tetragonal. Since the degenerate state is always split, no jump in $(T_1T)^{-1/2}$ takes place as x crosses into the tetragonal region.

Further evidence of hydrogen-vacancy splitting of the degenerate states can be inferred from the magnetic susceptibility measurements of the Ti-V-H system by Nagel *et al.*[35] Switendick[30] has indicated that a rigid-band description should be applicable for V substitution, raising the Fermi level in the TiH_2 density-of-states (DOS) diagram. With high enough vanadium concentrations, the Fermi level can be raised along the DOS diagram to energies beyond that of pure TiH_2. The data of Nagel *et al.* show two adjacent peaks as a function of V content and these are presumably the split states illustrated in Fig. 15(b). These peaks are further apart the less the hydrogen concentration, i.e., the greater the vacancy concentration. The two peaks remain at temperatures above where the tetragonal deformation takes place and are also seen to exist when the low-temperature data are extrapolated to the cubic phase. Thus we see that there is a splitting of the degenerate states even in the cubic phase which can be attributed to the vacancies.

One may also speculate that a vacancy splitting may result in the nonstoichiometry of these hydrides. As Switendick has shown, hydrogen-metal interaction brings metal states down below the Fermi level, thus lowering the energy. One might thus expect that the TiH_2 and ZrH_2 should be the most stable compounds. This, however, could be offset by a vacancy splitting of the degenerate band which would also lower the energy of occupied states. The nonstoichiometry indeed extends to the hydrogen concentration of $x=1.5$ where the Fermi level seems to lie at the beginning of the split band [near point A in Fig. 15(b).] A further decrease in concentration would place the Fermi level below the band and no energy reduction would be obtained by the splitting. In this context, one should note that V alloying reduces the nonstoichiometric range to $x=1.7$ instead of $x=1.5$.[41] Presumably V substitution may also break the symmetry and aid in the splitting. Thus not as many vacancies are needed to split the

degenerate states, raising the minimum nonstoichiometric range to $x=1.7$ instead of $x=1.5$. Reasoning along these lines may also explain why Azarkh *et al.*[24] obtained cubic rather than tetragonally deformed titanium hydrides in nonannealed samples. One may infer that annealing removes order-disturbing centers such as dislocations. These may disturb the symmetry and cause the energy-lowering degenerate band splitting, thus making a tetragonal distortion unnecessary in unannealed samples.

E. Metallurgical applications

Beck[27] first measured the hydrogen concentration dependence of microhardness in ZrH_x in order to prove that δ and ϵ are distinct phases rather than the δ phase simply being ϵ phase with $c/a=1$. Barraclough *et al.*[28] showed, however, that the microhardness changes continuously across the δ-ϵ interface (inset of Fig. 9). Thus one cannot attribute the abrupt change in microhardness to a change in phase. Neither can one correlate the microhardness behavior to the hydrogen concentration or unit-cell volume, since while these change monotonically across the entire concentration range, the microhardness at first decreases and then increases again. It is seen, however, from Fig. 9 that when $(T_1T)^{-1/2}$ (which is proportional to the DOS at the Fermi level) increases, microhardness decreases. At the concentration where $(T_1T)^{-1/2}$ has a peak, microhardness is minimum and then increases again when $(T_1T)^{-1/2}$ decreases. Thus it seems that there is an inverse correlation between the microhardness and the DOS at the Fermi level.

This observation can be of significance in metallurgical alloy design. For example, DOS calculations have been made for many metal systems (such as the hydrides) showing peaks and valleys in $N(E)$. While controversy exits as to whether the rigid-band model can be quantitatively relied on, there is general agreement that the Fermi level can be shifted to peaks or valleys in the DOS by alloying, as was demonstrated for example for the case of Ti-V-H by Nagel *et al.*[36] and Bowman *et al.*[5] If the correlation alluded to here is of general validity, it may be useful in designing alloys having desired mechanical properties.

V. CONCLUSIONS

We conclude the following.

(1) X-ray and NMR measurements of ZrH_x did not indicate a mixed $\delta+\xi$ region at the δ-ϵ phase boundary.

(2) A plateau is found in the variation of the unit-cell volume with hydrogen concentration over a small range of x where the tetragonal distortion begins.

(3) A peak in the DOS is obtained at hydrogen concentrations above that at which the tetragonal distortion occurs. Both the tetragonal distortion and the peak in the DOS occur at higher concentrations for TiH_x than for ZrH_x.

(4) The proton hyperfine interaction in TiH_x and ZrH_x is primarily due to core polarization with a hyperfine field of $H_{\rm hf}^{(d)}=-13.5$ kG.

(5) The concentration dependence of $(T_1T)^{-1/2}$ can be made to agree with Gupta's DOS band calculations. A sharp peak occurs at $ZrH_{1.80}$ and $TiH_{1.92}$ in the tetragonal phase.

(6) The concentration dependence of $(T_1T)^{-1/2}$ varies continuously while crossing the cubic-tetragonal transition region.

(7) The Switendick-Gupta description of the tetragonal deformation cannot be incorporated in a simple manner to explain the NMR and x-ray data in the nonstoichiometric compound. It is speculated that even at low enough hydrogen concentrations where the system is cubic the degenerate states are split by hydrogen vacancies and the Jahn-Teller distortion takes over when the vacancy concentration cannot support the splitting.

(8) A correlation between the microhardness and the DOS at the Fermi level $[(T_1T)^{-1/2}]$ was noted which indicates an inverse relationship between the two.

ACKNOWLEDGMENTS

I would like to thank Professor R. M. Cotts and Professor D. F. Holcomb for their hospitality and many helpful discussions. I am also grateful to the Laboratory of Atomic and Solid State Physics and the Materials Science Center of Cornell University for their financial support during the writing of this paper. I would also like to thank Batya Uzan for her technical assistance in the x-ray-diffraction measurements and Paul Newman for guiding me through the maze of the computer facility. The experimental portion of this study was performed at Ben Gurion University.

*Permanent address.

[1]H. L. Yakel Jr., Acta Crystallogr. 11, 46 (1958).

[2]C. Korn, Phys. Rev. B 17, 1707 (1978).

[3]C. Korn, in *Hydrides for Energy Storage—Proceedings of the International Symposium, Geilo, 1977,* edited by A. F. Andresen and A. J. Maeland (Pergamon, New York, 1978).

[4]R. Goring, R. Lucas, and K. Bohmhammel, J. Phys. C

14, 5675 (1981).
[5]R. C. Bowman, Jr. and W. K. Rhim, Phys. Rev. B 24, 2232 (1981).
[6]B. Nowak, O. J. Zogal and M. Minier, J. Phys. C 12, 4591 (1979).
[7]B. Stalinski, C. K. Coogan, and H. S. Gutowsky, J. Chem. Phys. 34, 1191 (1961).
[8]R. C. Frisch and A. Forman, J. Chem. Phys. 48, 5187 (1968).
[9]E. F. Khodosov and N. A. Shepilov, Phys. Status Solidi B 49, K83 (1972).
[10]A. E. Zweers, H. B. Brom, and W. J. Huiskamp, Physica 69, 336 (1973).
[11]I. A. Naskidashvili, Y. G. Sharimanov, N. Vilcu, D. Demco, and V. Simplaceanu, Fiz. Tverd. Tela (Leningrad) 19, 3465 (1977) [Sov. Phys.—Solid State 19, 2026 (1977)].
[12]K. R. Doolan, P. P. Narang, and J. M. Pope, J. Phys. F 10, 2073 (1980).
[13]J. M. Pope, P. P. Narang, and K. R. Doolan, J. Phys. Chem. Solids 42, 519 (1981).
[14]For a review, see A. C. Switendick, in *Hydrogen in Metals I,* Vol. 28 of *Topics in Applied Physics,* edited by G. Alefeld and J. Völkl (Springer, Berlin, 1978).
[15]N. I. Kulikov, V. N. Borzunov, and A. D. Zvonkov, Phys. Status Solidi B 86, 83 (1978).
[16]M. I. Darby, M. N. Read, and K. N. R. Taylor, Phys. Status Solidi B 102, 413 (1980).
[17]M. Gupta, Solid State Commun. 29, 47 (1979).
[18]M. Gupta, Phys. Rev. B 25, 1027 (1982).
[19]A. Fujimori and N. Tsuda, Solid State Commun. 41, 491 (1982).
[20]W. Trzebiatowsky and B. Stalinski, Bull. Acad. Polon. Sci. 1, 131 (1953).
[21]F. Ducastelle, R. Caudron, and P. Costa, J. Phys. (Paris) 31, 57 (1970).
[22]K. Bohmhammel, G. Wolf, G. Gross, and H. Madge, J. Low Temp. Phys. 43, 521 (1981).
[23]C. Korn and D. Zamir, J. Phys. Chem. Solids 31, 489 (1970).
[24]Z. M. Azarkh and P. I. Gavrilov, Sov. Phys.—Crystallogr. 15, 231 (1970) [Kristallografiya 15, 275 (1970)].
[25]J. C. MacDonald, J. Magn. Res. 38, 381 (1980).
[26]L. V. Azaroff and M. J. Buerger, *Powder Method in X-ray Crystallography* (McGraw-Hill, New York, 1958).
[27]R. L. Beck, Trans. ASM 55, 542 (1962).
[28]K. G. Barraclough and C. J. Beevers, J. Nucl. Mater. 34, 125 (1970).
[29]S. S. Sidhu, N. S. Satya Murthy, F. P. Campos, and D. D. Zauberis, Adv. Chem. Am. Chem. Soc. Ser. 39, 87 (1963).
[30]See, for example, A. Narath, in *Hyperfine Interactions,* edited by A. J. Freeman and R. B. Frankel (Academic, New York, 1967).
[31]A. C. Switendick, J. Less-Common Met. 49, 283 (1976).
[32]Y. Yafet and V. Jaccarino, Phys. Rev. 133, A1630 (1964).
[33]W. E. Blumberg, Phys. Rev. 119, 79 (1960).
[34]O. J. Zogal and S. Idziak, Physica 104B, 365 (1981).
[35]C. L. Wiley and F. Y. Fradin, Phys. Rev. B 17, 3462 (1978).
[36]H. Nagel and H. Goretzki, J. Phys. Chem. Solids. 36, 431 (1975).
[37]C. Korn, D. Zamir, and Z. Hadari, Acta Metall. 22, 33 (1974).
[38]A. C. Switendick, Z. Phys. Chem. 117, 447 (1979).
[39]E. Ehrenfreund, M. Weger, C. Korn, and D. Zamir, J. Chem. Phys. 50, 1907 (1969).
[40]L. F. Mattheiss and W. Weber, Phys. Rev. B 25, 2248 (1982).
[41]H. Nagel and R. S. Perkins, Z. Metallkunde 66, 362 (1975).